



A coherent image source method for sound prediction in long spaces with a sound absorbent ceiling

Hequn MIN¹; Yan CHEN²; Xiaojun QIU³

¹ Key Laboratory of Urban and Architectural Heritage Conservation, Ministry of Education, School of Architecture, Southeast University, China

² Institute of Acoustics and Key Laboratory of Modern Acoustics of MOE, Nanjing University, China

³ Institute of Acoustics and Key Laboratory of Modern Acoustics of MOE, Nanjing University, China

ABSTRACT

Sound absorbing boundaries can attenuate noise propagation in a long space, but they may lead the sound field hard to be accurately predicted. This paper presents a coherent image source model for sound field in long spaces with a sound absorbing ceiling. In this model, the reflections on the absorbent boundary are separated from those on reflective ones during applying reflection coefficients. The model is compared with the classic wave theory, the existing coherent ray-based model and a scale-model experiment. The results show that the proposed model has considerable accuracy and distinct advantage over the existing model for sound prediction in long spaces with an absorbent ceiling.

Keywords: image source method, long space, sound absorption I-INCE Classification of Subjects Number(s): 51.1.3

1. INTRODUCTION

For noise control in many practical long spaces such as traffic tunnels and subway stations, it is often the case to apply acoustical liners to the space ceiling for larger noise attenuation. Regarding sound prediction in such spaces, sound field is not diffuse so that classic room acoustics formulas are inapplicable [1,2]. And the usual energy-based (incoherent) geometrical acoustics models^{3, 4} cannot account for the interference between multiple sound reflections and the reflection phase changes on impedance boundaries. Those phenomena were experimentally observed to be distinct in this situation [2,5,6] and can notably affect the sound prediction accuracy, especially at lower frequencies and in early part of the impulse response [6]. As for the wave-based (coherent) geometrical acoustics models, Li *et al.* developed a numerical model for coherent sound prediction inside long spaces [2], and afterwards applied this prediction model into full-scale tunnels [5] and a long space with impedance discontinuities [7]. It was shown that their coherent prediction model provides much better prediction accuracy than the usual incoherent ones for long spaces with reflective boundaries. However for applications with sound absorbing boundaries, applicability of their model may still stay limited. It's because their model originates from a coherent image source method by Lemire and Nicolas [8], in which it is implicitly assumed that the wave front shapes remain spherical during each successive reflection of the initial spherical wave radiation [8]. This assumption may hardly hold for reflections upon sound absorbing boundaries.

Recently, Min *et al.* [9] proposed a coherent image source method for fast yet accurate sound prediction in flat spaces with absorbent boundaries. They separated reflections on the absorbent boundary from those on reflective ones during applying reflection coefficients, which avoids the prediction difficulties with absorbent boundaries in the method of Lemire and Nicolas. Unfortunately, in theory, their model is currently limited to spaces with two parallel infinite boundaries. It is the intent of this work to extend their model for fast yet accurate sound prediction in practical long spaces with

¹ hqmin@seu.edu.cn

² ychen@nju.edu.cn

³ xjqiu@nju.edu.cn

sound absorbing boundaries, initially in a long rectangular space with a sound absorbing ceiling.

2. COHERENT IMAGE SOURCE MODEL

Figure 1 shows cross section geometry of a long rectangular space with a height of H and width W . For simplicity, four boundaries in this space, the ceiling, ground, right and left walls, are assumed to be geometrically reflecting and locally reactive with a uniform normalized specific admittance of β_c , β_g , β_r , and β_l , respectively. In this paper, the ceiling is defined to be sound-absorptive with relatively high β_c , while other boundaries are sound-reflective with relatively low admittances. The space extends infinitely along the y -direction as a typical case and a point source is defined at $(x_s, 0, z_s)$ and receiver at (x, y, z) inside.

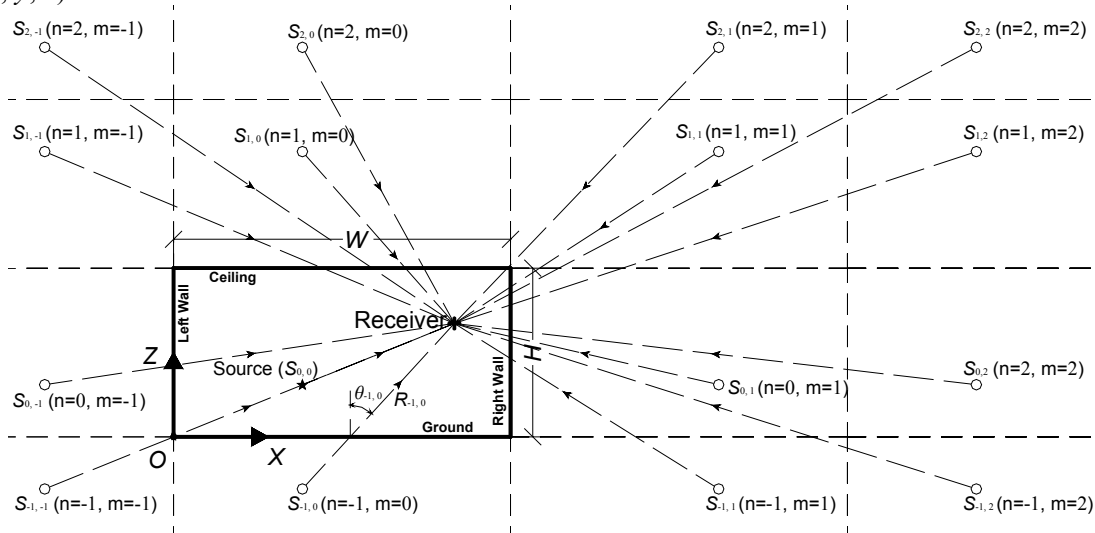


Figure 1 – Cross section geometry of a long rectangular space and the image sources formed by multiple reflections on four boundaries of ceiling, ground, right and left walls, respectively. The space is with the height H and width W , and extends along the y -direction.

For the sound field modeling, we first assume that $kW \gg 1$ and $kH \gg 1$ (with k for the wavenumber) so that the boundaries may be considered as infinity for each sound reflection on them [8]. It is also assumed that both the source and receiver are far away from any interaction corner of boundaries compared to the wavelength so that the sound diffraction at corners can be neglected by comparison to the boundary reflections [10,11]. Then the total sound field at the receiver in this space can be approximated as summation of successive sound reflections on four boundaries,

$$P_{tot} \approx \sum_{n=-\infty}^{+\infty} \sum_{m=-\infty}^{+\infty} P_{n,m} \quad (1)$$

where $n, m = 0, \pm 1, \pm 2, \dots$, and $P_{n,m}$ represents the sound field contribution from the (n, m) -th order image source, in which a positive n (or m) is for an image source located above the ceiling (or rightwards from the right wall) while a negative n (or m) is for that located below the floor (or leftwards from the left wall), as shown in Figure 1. Particularly, $P_{0,0}$ denotes the direct sound from the real source $S_{0,0}$. $P_{-1,0}$ represents the single sound reflection on the ground, and based on the assumptions above, it can be approximated from the plane wave expansion of a spherical wave as [9,12]

$$P_{-1,0} \approx \frac{jk}{8\pi^2} \int_0^{2\pi} \int_0^{\pi-j\infty} e^{jk \cdot \mathbf{R}_{-1,0}} V_g(\theta) \sin \theta d\theta d\varphi \quad (2)$$

where \mathbf{k} is the wave number vector $k(\sin\theta\cos\varphi, \sin\theta\sin\varphi, \cos\theta)$, and θ and φ are azimuth angles used to describe the propagation direction of each elementary plane wave in vertical (x - z) and horizontal (x - y) planes, respectively. $\mathbf{R}_{-1,0} = (R_{-1,0}\sin\theta_{-1,0}\cos\varphi_{-1,0}, R_{-1,0}\sin\theta_{-1,0}\sin\varphi_{-1,0}, R_{-1,0}\cos\theta_{-1,0})$ denotes the distance vector from the image source $S_{-1,0}$ to the receiver with explicit azimuth angles $\theta_{-1,0}$ and $\varphi_{-1,0}$, as shown in Figure 1. $V_g(\theta)$ is the plane wave reflection coefficient on the “infinite” ground with the incidence angle θ ,

$$V_g(\theta) = \frac{\cos\theta - \beta_g}{\cos\theta + \beta_g}. \quad (3)$$

Based on Eq. (2), $P_{n,m}$ can be evaluated accordingly [9]

$$P_{n,m} \approx \frac{jk}{8\pi^2} \int_0^{2\pi} \int_0^{\frac{\pi}{2}-j\infty} e^{jk \cdot \mathbf{R}_{n,m}} [V_g(\theta)]^{n_g} [V_c(\theta)]^{n_c} [V_l(\alpha)]^{m_l} [V_r(\alpha)]^{m_r} \sin\theta \, d\theta \, d\varphi, \quad (4)$$

where n_g , n_c , m_l and m_r are used to count reflection times on the ground, ceiling, left and right wall in the path from $S_{n,m}$ to the receiver, respectively. They can be determined from the order (n, m) by

$$n_g = \frac{|n|}{2} - \frac{1}{2} \text{sign}(n) \text{rem}(|n|, 2), \quad (5a)$$

$$n_c = \frac{|n|}{2} + \frac{1}{2} \text{sign}(n) \text{rem}(|n|, 2), \quad (5b)$$

$$m_l = \frac{|m|}{2} - \frac{1}{2} \text{sign}(m) \text{rem}(|m|, 2), \quad (5c)$$

and

$$m_r = \frac{|m|}{2} + \frac{1}{2} \text{sign}(m) \text{rem}(|m|, 2), \text{ respectively.} \quad (5b)$$

In Eq. (4), $\mathbf{R}_{n,m} = (R_{n,m} \sin\theta_{n,m} \cos\varphi_{n,m}, R_{n,m} \sin\theta_{n,m} \sin\varphi_{n,m}, R_{n,m} \cos\theta_{n,m})$ represents the distance vector from $S_{n,m}$ to the receiver, with explicit azimuth angles $\theta_{n,m}$ and $\varphi_{n,m}$. $V_c(\theta)$ is the plane wave reflection coefficient on the ceiling with the incidence angle θ , while $V_l(\alpha)$ and $V_r(\alpha)$ are those on the left and right walls with the incidence angle $\alpha = \pi/2 - \theta$, respectively. Evaluation of $V_c(\theta)$, $V_l(\alpha)$ and $V_r(\alpha)$ is similar to $V_g(\theta)$ in Eq. (3). Through an identical mathematical transformation similar to that from Eq. (8) to Eq. (12) in Ref. 7.3, the sound field contribution of $P_{n,m}$ in Eq. (4) can be further simplified as

$$P_{n,m} \approx \frac{jk}{8\pi} \int_{\frac{\pi}{2}+j\infty}^{\frac{\pi}{2}-j\infty} V(\theta) \sin\theta \cdot H_0^1(kr \sin\theta) e^{jkR_{n,m} \cos\theta \cos\theta_{n,m}} \, d\theta, \quad (6)$$

where $V(\theta)$ represents an overall reflection coefficient equal to the term $[V_g(\theta)]^{n_g} [V_c(\theta)]^{n_c} [V_l(\alpha)]^{m_l} [V_r(\alpha)]^{m_r}$, $r = R_{n,m} \sin\theta_{n,m}$, and $H_0^1(\cdot)$ is the first kind Hankel function with the zero-th order.

For the evaluation of $P_{n,m}$ in Eq. (6), the ray field from single reflection on the reflective boundaries, $P_{-1,0}$ for example, can be further evaluated as [8, 13]

$$P_{-1,0} = Q_{ref}(S_{-1,0}, R | GB) \cdot \frac{e^{jkR_{-1,0}}}{4\pi R_{-1,0}}, \quad (7)$$

where $Q_{ref}(S_{-1,0}, R | GB)$ represents the single reflection coefficient on the reflective ground boundary (GB) and can be evaluated as [8, 13]

$$Q_{ref}(S_{-1,0}, R | GB) = V_g(\theta_{-1,0}) + [1 - V_g(\theta_{-1,0})] F(w_n), \quad (8)$$

in which

$$F(w_n) = 1 + j\sqrt{\pi} \cdot w_n \cdot g(w_n), \quad (9)$$

$$w_n = \sqrt{kR_{-1,0}} \cdot \frac{1+j}{2} \cdot (\cos\theta_{-1,0} + \beta_g), \text{ and} \quad (10)$$

$$g(w_n) = e^{-w_n^2} \text{erfc}(jw_n). \quad (11)$$

When real part of $w_n > 3$, or image part of $w_n > 2$, or any one of these two parts ≤ 6 , $g(w_n)$ can be approximated as [14]

$$g(w_n) \approx -jw_n \left[\frac{0.4613135}{w_n^2 - 0.1901635} + \frac{0.09999216}{w_n^2 - 1.7844927} + \frac{0.002883894}{w_n^2 - 5.5253437} \right], \quad (12)$$

and when real or image part of $w_n > 6$,

$$g(w_n) \approx -jw_n \left[\frac{0.5124242}{w_n^2 - 0.275255} + \frac{0.05176536}{w_n^2 - 2.724745} \right]. \quad (13)$$

It was shown that the wave front shape before and after each reflection on the reflective boundaries can almost keep the same [9, 15]. This suggests that, single reflection coefficients Q_{ref} shall be weakly dependant on θ and be almost uniform for different spatial parts of incident wave fronts with any shapes [9]. That is, during the ray propagation from $S_{n,m}$ to receiver in Figure 1, evaluation of each reflection upon one reflective boundary (or each “transmission” through it or its images) can be simplified by weighting the corresponding perfect reflection from the incident wave with the single reflection coefficient Q_{ref} on this boundary [9]. Thus after the ray field being weighted for n_g , m_l and m_r times due to “transmission” through the reflective ground, left wall (LW) and right wall (RW) or their images, respectively, $P_{n,m}$ can be much simplified as

$$P_{n,m} \approx [Q_{ref}(S_{n,m}, R | GB)]^{n_g} \cdot [Q_{ref}(S_{n,m}, R | LW)]^{m_l} \cdot [Q_{ref}(S_{n,m}, R | RW)]^{m_r} \cdot \frac{jk}{8\pi} \int_{\frac{\pi}{2} + j\infty}^{\frac{\pi}{2} - j\infty} [V_c(\theta)]^{n_c} \sin \theta \cdot H_0^1(kr \sin \theta) e^{jkR_{n,m} \cos \theta \cos \theta_{n,m}} d\theta, \quad (14)$$

where the integral involves only the reflection coefficient on the absorptive ceiling and can be further evaluated through the second order approximation in Eq. (16) of Ref. 9 to yield

$$P_{n,m} \approx [Q_{ref}(S_{n,m}, R | GB)]^{n_g} \cdot [Q_{ref}(S_{n,m}, R | LW)]^{m_l} \cdot [Q_{ref}(S_{n,m}, R | RW)]^{m_r} \cdot \left\{ V_t(\theta_{n,m} | CB, n_c) - \frac{j[V_t'(\theta_{n,m} | CB, n_c) \cot \theta_{n,m} + V_t''(\theta_{n,m} | CB, n_c)]}{2kR_{n,m}} \right\} \cdot \frac{ejkR_{n,m}}{4\pi R_{n,m}}, \quad (15)$$

with $V_t(\theta_{n,m} | CB, n_c) = [V_c(\theta_{n,m})]^{n_c}$. This equation may be rewritten as one typical image source model form,

$$P_{n,m} = Q_{n,m} \frac{e^{jkR_{n,m}}}{4\pi R_{n,m}}, \quad (16)$$

where $Q_{n,m}$ represents a combined reflection coefficient corresponding to the ray with reflection order (n,m)

$$Q_{n,m} = [Q_{ref}(S_{n,m}, R | GB)]^{n_g} \cdot [Q_{ref}(S_{n,m}, R | LW)]^{m_l} \cdot [Q_{ref}(S_{n,m}, R | RW)]^{m_r} \cdot Q_{abs}(S_{n,m}, R | CB, n_c), \quad (17)$$

in which $Q_{abs}(S_{n,m}, R | CB, n_c)$ represents one reflection coefficient accounting for overall effect from successive reflections on the absorptive ceiling boundary (CB) as

$$Q_{abs}(S_{n,m}, R | CB, n_c) \approx V_t(\theta_{n,m} | CB, n_c) - \frac{j[V_t'(\theta_{n,m} | CB, n_c) \cot \theta_{n,m} + V_t''(\theta_{n,m} | CB, n_c)]}{2kR_{n,m}}. \quad (18)$$

Eqs. (16) to (18) provide an extension of the coherent image source method in Ref. 9 into long rectangular spaces with a sound absorbent ceiling.

3. NUMERICAL RESULTS AND DISCUSSION

Numerical simulations are firstly conducted to investigate prediction performance with the proposed coherent image source model. As the classic wave theory [16] can be analytically exact in spaces focused in this paper, it is used as a reference method to provide benchmark results for numerical validations. The widely used existing coherent image source method by Lemire and Nicolas [8] is also investigated for comparisons. The numerical implementation of the image source methods and the wave theory stays similar to that in Refs. [8] and [9], except the geometry of four boundaries in Figure 1. In numerical investigations, a long rectangular space with $W \times H = 20\text{m} \times 5\text{m}$ is considered to simulate one actual city road tunnel with four lanes. For simplification, four tunnel boundaries are all assumed to be rigidly backed layers of homogeneous porous material. Attenborough's “three-parameter” approximation¹⁷ is applied to evaluate surface admittances for the tunnel

boundaries, in which boundary media parameters of flow resistivity (σ), porosity (Ω), tortuosity (T), pore shape factor (S_p) and thickness (d) are used for description. The tunnel ceiling is defined to be highly sound absorptive with $\sigma=10$ cgs (where $1 \text{ cgs}=1 \text{ kPa s m}^{-2}$), $\Omega=1$, $T=1$, $S_p=0.25$ and $d=0.1$ m, such as a wool layer. The ground is with $\sigma=10\text{k}$ cgs, $\Omega=0.2$, $T=1.4$, $S_p=0.5$ and $d=0.05$ m to represent a compacted asphalt pavement layer. The right and left walls are with $\sigma=0.5\text{k}$ cgs, $\Omega=0.1$, $T=1$, $S_p=0.3$ and $d=0.01$ m to represent cement plaster over concrete walls. Figure 2 shows the corresponding normal incident absorption coefficients of these four boundaries in the numerical case.

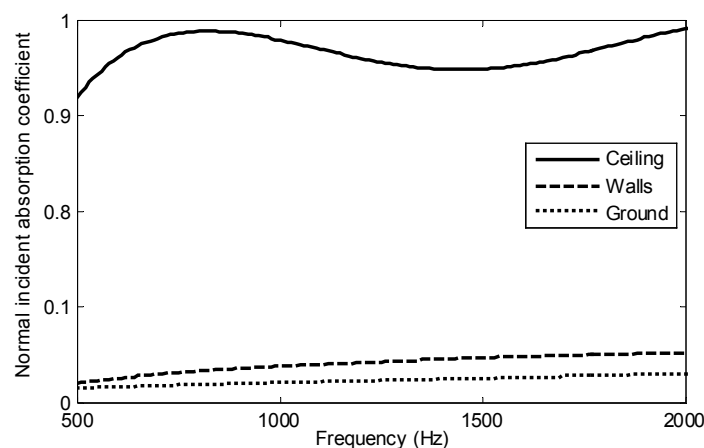


Figure 2 – Spectra of normal incident absorption coefficient on four boundaries of the rectangular long space in numerical simulations.

Two sets of numerical simulations are conducted. In the first set, predictions of sound pressure level (SPL) spectrum at receiver (6 m, 50 m, 1 m) from a point source at (6 m, 0, 1 m) are investigated in the numerical case. Results from the proposed method, the wave theory and the method of Lemire and Nicolas⁸ are compared in Figure 3. It is shown that, results from the proposed method agree excellently with those of the wave theory over frequencies from 500 to 2000 Hz, except small deviations (< 1 dB) at few lower frequencies. By contrast however, predictions with the method of Lemire and Nicolas differ significantly from the benchmark results over frequencies in this situation. This validates the successful extension of the coherent image source method by Min *et al.* [9] for spaces enclosed by four perpendicular finite boundaries in this paper. It also indicates that the existing coherent models based on the method of Lemire and Nicolas can hardly have accurate predictions in long spaces with absorptive boundaries, because the assumption of spherical wave front shapes for each successive reflection can not be satisfied in this situation. The computational time in this set of simulations is also compared. All simulations are executed in Matlab 2010b on a same personal computer with a 2.4 GHz Intel Core i5-560M processor and 8 Gbytes of random access memory. Records show that, for results at all the 31 frequencies in Figure 3, evaluation of the proposed model and the method of Lemire and Nicolas takes 50.3 s and 49.7 s, respectively, while the corresponding execution time with the wave theory takes over 2 hours. This shows the remarkable advantage of the proposed model both at accuracy and efficiency for sound predictions in long spaces with absorptive boundaries.

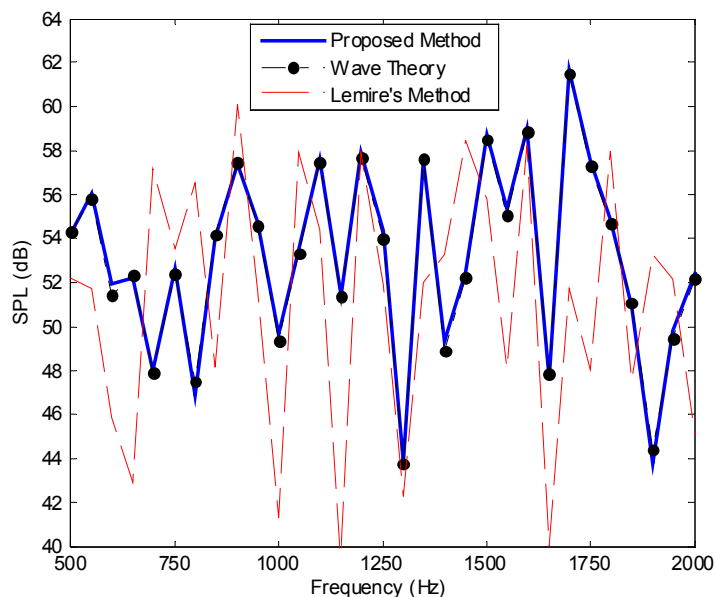


Figure 3 – Comparison of predictions on sound pressure level (SPL) spectrum in a long space with 20 m wide and 5 m high in numerical simulations. The source is located at (6, 0, 1) m and the receiver at (6, 50, 1) m.

Second, predictions of the SPL distribution inside the long rectangular space are investigated in the numerical case. Figure 4 presents predicted SPL results at frequency of 1000 Hz versus the receiver location along the tunnel extension direction. The source is located at (6 m, 0, 1 m) and the receiver at (6 m, y_r , 1 m) with y_r moving from 5 m to 200 m. From Figure 2, the absorption coefficients of the ceiling, ground, and walls at frequency of 1000 Hz are 0.98, 0.02 and 0.04, respectively. Results in Figure 4 show remarkably good agreement between the proposed model and the wave theory, even at receiver locations far away from the source compared to the space height and width. However large prediction differences can be always seen between the method of Lemire and Nicolas and the benchmark method in this situation, even at locations near the source. Figure 4 also shows that prediction error from the proposed method increases at a longer distance between the source and receiver. The reason may be that, when receiver moves farther away from the source compared to the space cross section dimensions, high-order reflection rays provide higher relative contributions in the total sound field in Eq. (1). From the proposed model, reflection ray field is evaluated by Eq. (14) through approximating each reflection at reflective boundaries as one single reflection. This unavoidably introduces and accumulates larger errors for higher-order reflection rays and the total field at farther locations from the source. Figure 5 presents the SPL predictions at frequency of 1000 Hz versus the receiver location along the tunnel width direction. The source is located at (6 m, 0, 1 m) as well and the receiver at (x_r , 50 m, 1 m) with x_r moving from 1 m to 19 m. Results show excellent prediction agreement between the propose model and the wave theory as well, even at receiver locations close to the interaction corner compared to the wavelength. This suggests that the assumption of source and receiver staying far away from interaction corners of boundaries may be relaxed in applying the proposed model. In Figure 5, large discrepancies remain between the method of Lemire and Nicolas and the benchmark method still. Predictions are also compared on the SPL at 1000 Hz versus the receiver location along the tunnel height direction, with the source at (6 m, 0, 1 m) and receiver at (6 m, 50 m, z_r) m with z_r moving from 0.125 m to 4.875 m. The corresponding results are presented in Figure 6. It is shown that results from the proposed model can almost overlap those from the wave theory, but only at receiver locations very close to the reflective ground but at those in the vicinity of the absorbent ceiling compared to the wavelength. Predictions with the method of Lemire and Nicolas still go far from the benchmark results in this situation. These results in the numerical case suggests that, the extended coherent image source model can accurately predict the sound fields in long rectangular spaces with an absorbent ceiling, while its computational efficiency stays at a same level with the existing coherent ray-based models.

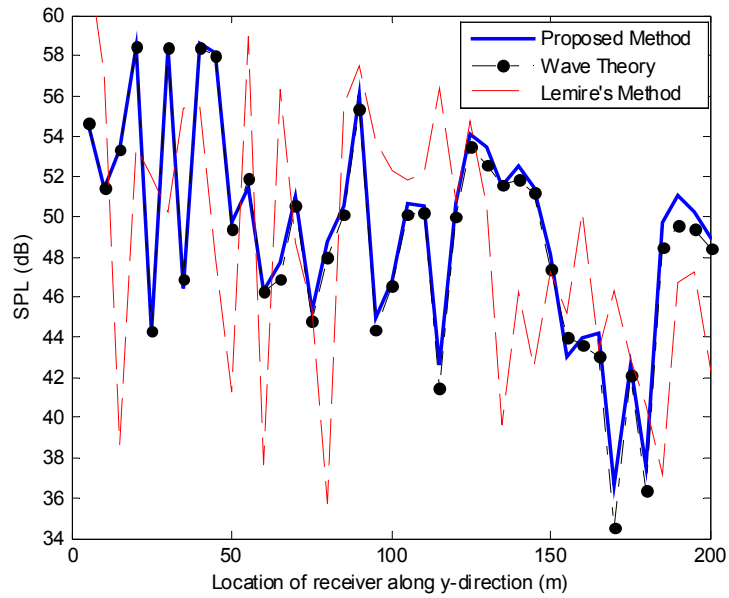


Figure 4 – Comparison of SPL predictions at frequency of 1000 Hz vs. receiver location along y -direction. The source is located at (6 m, 0, 1 m) and the receiver at (6 m, y_r , 1 m) with y_r moving from 5 m to 200 m.

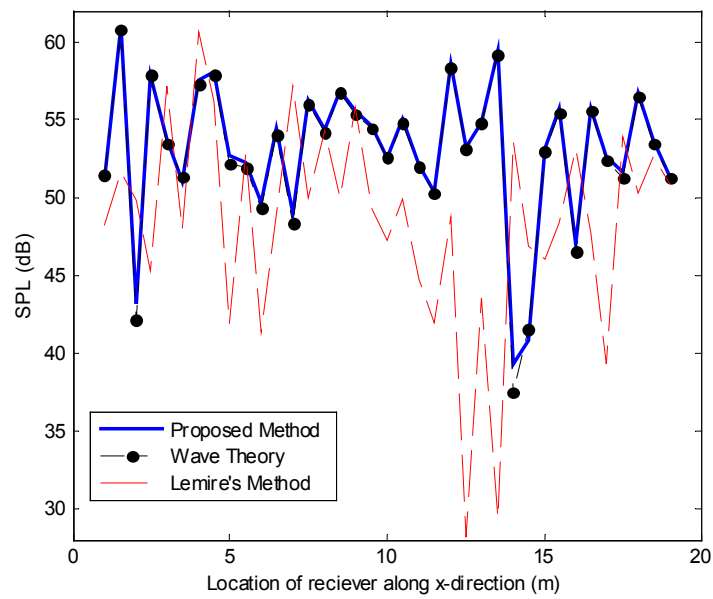


Figure 5 – Comparison of SPL predictions at frequency of 1000 Hz vs. receiver location along x -direction. The source is located at (6 m, 0, 1 m) and the receiver at (x_r , 50 m, 1 m) with x_r moving from 1 m to 19 m.

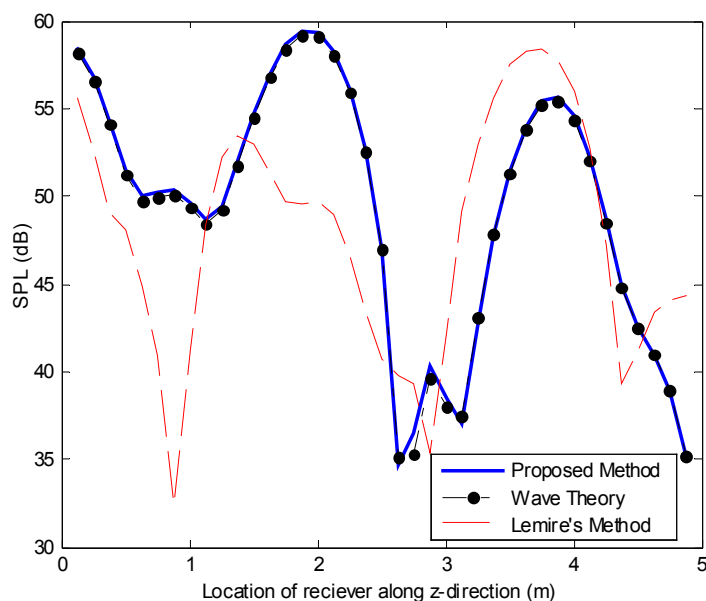


Figure 6 –Comparison of SPL predictions at frequency of 1000 Hz vs. receiver location along z -direction. The source is located at (6 m, 0, 1 m) and receiver at (6 m, 50 m, z_r) with z_r moving from 0.125 m to 4.875 m.

4. CONCLUSION

In this paper, an extended coherent image source model is proposed for simple yet accurate sound prediction in long rectangular spaces with a sound absorbing ceiling. Prediction from the proposed model has been compared with that from the wave theory and that from an existing coherent ray-based method. It is shown that the proposed model can fast yet accurately predict the sound propagation in long rectangular spaces with an absorbent ceiling at frequencies not too low, with remarkable advantages over the existing coherent ray-based models.

ACKNOWLEDGEMENTS

This work is supported by the Natural Science Foundation of China (Grant No. 51408113) and the Natural Science Foundation of Jiangsu Province, China (Grant No. BK20140632).

REFERENCES

1. Kang J. The unsuitability of the classic acoustical theory in long enclosures. *Architect Sci Rev.* 1996; 39: 89–94.
2. Li KM, Iu KK. Propagation of sound in long enclosures. *J Acoust Soc Am.* 2004; 116: 2759–2770.
3. Kang J. A method for predicting acoustic indices in long enclosures. *Appl Acoust.* 1997; 51: 169–180.
4. Yang L, Shield BM. The prediction of speech intelligibility in underground stations of rectangular cross section. *J Acoust Soc Am.* 2001; 109: 266–273.
5. Li KM, Iu KK. Full-scale measurements for noise transmission in tunnels. *J Acoust Soc Am.* 2005; 117: 1138–1145.
6. Yousefzadeh B, Hodgson M. Energy- and wave-based beam-tracing prediction of room-acoustical parameters using different boundary conditions. *J Acoust Soc Am.* 2012; 132: 1450–1461.
7. Lam PM, Li KM. A coherent model for predicting noise reduction in long enclosures with impedance discontinuities. *J Sound Vib.* 2007; 299: 559–574.
8. Lemire G, Nicolas J. Aerial propagation of spherical sound waves in bounded spaces. *J Acoust Soc Am.* 1989; 85: 1845–1853.
9. Min H, Chen W, Qiu X. Single frequency sound propagation prediction in flat waveguides with locally reactive impedance boundaries. *J Acoust Soc Am.* 2011; 130: 772–782.
10. Hadden WJ, Pierce AD. Sound diffraction around screens and wedges for arbitrary point source location. *J Acoust Soc Am.* 1981; 69: 1266–1276.
11. Min H, Qiu X. Multiple acoustic diffraction around rigid parallel wide barriers. *J Acoust Soc Am.* 2009;

- 126: 179-186.
12. Brekhovskikh I. *Waves in Layered Media*, 2nd ed. New York: Academic; 1980. p. 225-320.
 13. Attenborough K, Hayek SI, Lawther JM. Propagation of sound above a porous half space. *J Acoust Soc Am*. 1980; 68: 1493-1501.
 14. Abramowitz M, Stegun IA. *Handbook of Mathematical Functions with Formulas, Graphs, and Mathematical Tables*. New York : Dover; 1965. p. 328.
 15. Ingard U. On the reflection of a spherical sound wave from an infinite plane. *J Acoust Soc Am*. 1951; 23: 329-335.
 16. Morse PM, Ingard KU. *Theoretical Acoustics*. New York: McGraw-Hill; 1968. p. 492-509.
 17. Attenborough K. Ground parameter information for propagation modeling. *J Acoust Soc Am*. 1992; 92: 418-427.